Structural Characterization of the Proximal and Distal Histidine Environment of Cytoglobin and Neuroglobin

Hitomi Sawai,[‡,§] Masatomo Makino,[‡,§] Yasuhisa Mizutani,[∥] Takehiro Ohta,[⊥] Hiroshi Sugimoto,[§] Tadayuki Uno,[@] Norifumi Kawada,[#] Katsutoshi Yoshizato,[+] Teizo Kitagawa,[⊥] and Yoshitsugu Shiro*[,§]

Department of Life Science, Graduate School of Science, Himeji Institute of Technology/University of Hyogo, 3-2-1 Kouto, Kamigori-cho, Ako, Hyogo 678-1297, Japan, RIKEN Harima Institute/SPring-8, 1-1-1 Kouto, Mikazuki-cho, Sayo, Hyogo 679-5148, Japan, Molecular Photoscience Research Center, Kobe University, 1-1 Rokkodai, Nada-ku, Kobe 657-8501, Japan, Center for Integrative Bioscience, Okazaki National Research Institutes, Myodaiji, Okazaki, Aichi 444-8787, Japan, Graduate School of Pharmaceutical Sciences, Osaka University, 1-6 Yamada-oka, Suita, Osaka 565-0871, Japan, Department of Hepatology, Graduate School of Medicine, Osaka City University, 1-4-3 Asahi-machi, Abeno-ku, Osaka 545-8585, Japan, Developmental Biology Laboratory and 21st Century COE Program for Advanced Radiation Casualty Medicine, Department of Biological Science, Graduate School of Science, Hiroshima University, 1-3-1 Kagamiyama, Higashihiroshima, Hiroshima 739-8526, Japan, and Yoshizato Project, Cooperative Link of Unique Science and Technology for Economy Revitalization (Japan Science and Technology Organization), Hiroshima Prefectural Institute of Industrial Science and Technology, 3-10-32, Kagamiyama, Higashihiroshima, Hiroshima 739-006, Japan

Received May 27, 2005; Revised Manuscript Received August 1, 2005

ABSTRACT: Cytoglobin (Cgb) and neuroglobin (Ngb) are the first examples of hexacoordinated globins from humans and other vertebrates in which a histidine (His) residue at the sixth position of the heme iron is an endogenous ligand in both the ferric and ferrous forms. Static and time-resolved resonance Raman and FT-IR spectroscopic techniques were applied in examining the structures in the heme environment of these globins. Picosecond time-resolved resonance Raman (ps-TR^3) spectroscopy of transient five-coordinate heme species produced by the photolysis of carbon monoxide (CO) adducts of Cgb and Ngb showed Fe−His stretching (ν_{Fe-His}) bands at 229 and 221 cm^{-1}, respectively. No time-dependent shift in the ν_{Fe-His} band of Cgb and Ngb was detected in the 20−1000 ps time domain, in contrast to the case of myoglobin (Mb). These spectroscopic data, combined with previously reported crystallographic data, suggest that the structure of the heme pocket in Cgb and Ngb is altered upon CO binding in a manner different from that of Mb and that the scales of the structural alteration are different for Cgb and Ngb. The structural property of the heme distal side of the ligand-bound forms was investigated by observing the sets of (ν_{Fe-CO}, ν_{C-O}, δ_{Fe-C-O}) and (ν_{Fe-NO}, ν_{N-O}, δ_{Fe-N-O}) for the CO and nitric oxide (NO) complexes of Cgb and Ngb. A comparison of the spectra of some distal mutants of Cgb (H81A, H81V, R84A, R84K, and R84T) and Ngb (H64A, H64V, K67A, K67R, and K67T) showed that the CO adducts of Cgb and Ngb contained three conformers and that the distal His (His81 in Cgb and His64 in Ngb) mainly contributes to the interconversion of the conformers. These structural characteristics of Cgb and Ngb are discussed in relation to their ligand binding and physiological properties.

Heme-containing globin proteins are widely distributed in biological systems, including bacteria, fungi, protists, plants, and animals (*1*). In vertebrates, tetrameric hemoglobin (Hb)[1] present in erythrocytes plays a role in supplying oxygen (O_2) to the body (*2*), while monomeric and muscle-specific myoglobin (Mb) serves as a sourse of intracellular O_2 storage to possibly enhance the diffusion of O_2 to the mitochondria and/or is presumably involved in the detoxification of NO (*3*). In addition to Hb and Mb, two novel members, neuroglobin (Ngb) (*4*) and cytoglobin (Cgb) (*5*−*7*), have recently been added to the vertebrate globin family. Cgb is also known as the stellate cell activation-associated protein (STAP) (*6*, *7*) or histoglobin (*9*). This protein is present in virtually all tissues. On the other hand, Ngb is present in cells of the vertebrate central and peripheral nervous system, the retina (*8*), and also endocrine tissue (*4*). The primary sequences of Cgb and Ngb are only distantly related to Hb and Mb, the level of identity being ∼25%, but some amino acid residues are highly conserved in the vertebrate globin family (*10*). Since the conserved residues of Mb and Hb are located around the heme active sites and are important in the binding of external ligands to the heme iron, it has been suggested that Ngb and Cgb are possibly involved in the binding of O_2 in the distributed cells. Although the physi-

* To whom correspondence should be addressed. Telephone: +81-791-58-2817. Fax: +81-791-58-2818. E-mail: yshiro@riken.jp.
‡ Himeji Institute of Technology/University of Hyogo.
§ RIKEN Harima Institute/SPring-8.
∥ Kobe University.
⊥ Okazaki National Research Institutes.
@ Osaka University.
# Osaka City University.
+ Hiroshima University and Hiroshima Prefectural Institute of Industrial Science and Technology.

[1] Abbreviations: Cgb, cytoglobin; Ngb, neuroglobin; Mb, myoglobin; Hb, hemoglobin; TR^3, time-resolved resonance Raman; FT-IR, Fourier transform infrared; CO, carbon monoxide; NO, nitric oxide; ν_{Fe-His}, Fe−His stretching mode.

10.1021/bi050997o CCC: $30.25
Published on Web 09/13/2005

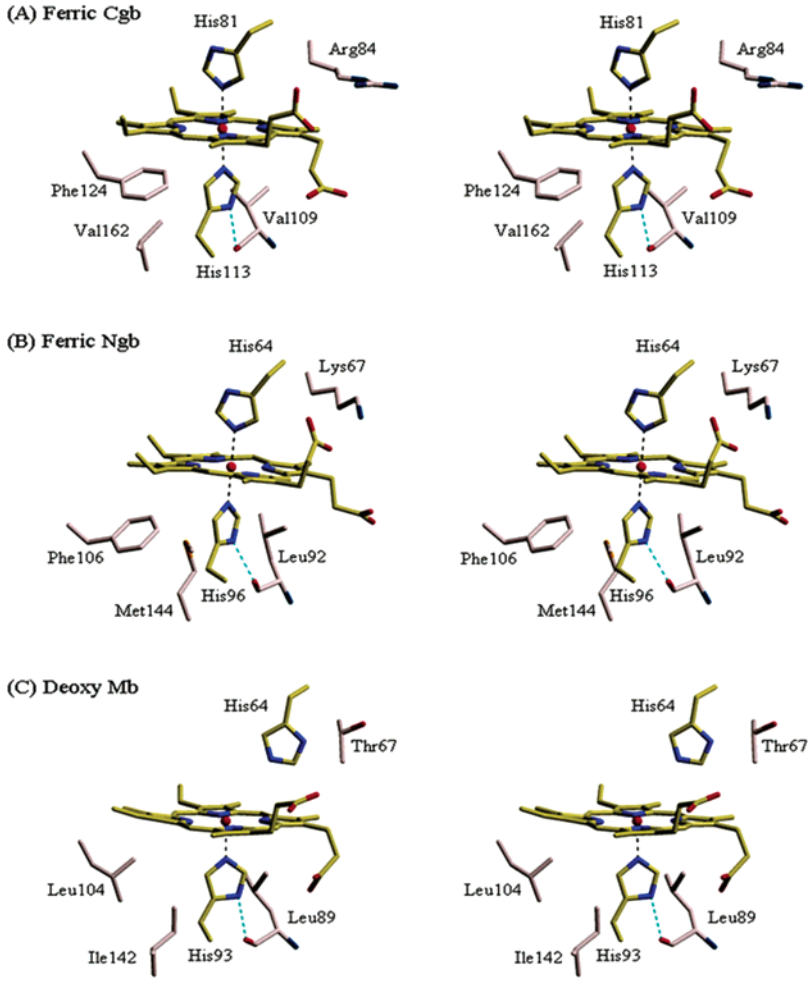

FIGURE 1: Stereoviews showing selected residues surrounding the heme for (A) the ferric form of Cgb (*16*), (B) the ferric form of Ngb (*14*), and (C) the deoxy form of SWMb. These figures were drawn using the atomic coordinates from PDB entries 1V5H, 1OJ6, and 1A6N, respectively, and were created with MOLSCRIPT (*46*) and Raster3D (*47*). The coloring is by residue [the heme and the axial residues (khaki) and other residues (gray)], by atom type [O and Fe (red) and N (blue)], and by bond type [hydrogen bond with the proximal His (cyan) and coordinate bond with the axial His (black)].

ological roles of Ngb and Cgb are poorly understood at present, plausible hypotheses of their functions have been proposed; they might act as temporary oxygen storage proteins and/or a scavenger of bioactive compounds (e.g., NO, peroxynitrite, and hydrogen peroxide) in hypoxic cells, since the expression of both proteins appears to be upregulated in hypoxia (*11*, *12*). In addition, it was revealed that oxyNgb reacts very rapidly with NO, yielding metNgb and NO_3^- by means of a heme-bound peroxynitrite intermediate (*13*).

Most recently, crystal structures of Cgb and Ngb in the ferric state have been reported (*14*−*17*). Both consist of eight α-helices and exhibit a typical globin fold with a "three-over-three α-helical sandwich". As in the case for Hb and Mb, the heme of Cgb and Ngb is embedded between the E and F helices, and the histidyl imidazole (His113 in Cgb and His96 in Ngb) coordinates to the heme iron as a fifth axial ligand. However, their coordinated hemes have a significant characteristic structure, in that the sixth coordination position of the heme iron atom is occupied by the histidyl imidazole, His81 in Cgb and His64 in Ngb, indicating that the heme iron in these globins is in a bis-His hexacoordination (*18*, *19*) as shown in Figure 1. Spectroscopic studies support this coordination structure of the heme iron for Cgb and Ngb in the ferric state, and also indicate a hexacoordination structure, even in the deoxygenated ferrous form (*6*, *20*). The findings are in sharp contrast to the pentacoordinated structure of the deoxygenated ferrous heme iron of Hb and Mb.

The endogenous sixth ligand, His81 for Cgb and His64 for Ngb, is replaced by exogenous ligands such as O_2, CO, and NO, to yield a "new" hexacoordinated heme iron in the ferrous low-spin state, as has been shown in previous kinetic, spectroscopic, and mutational studies (*18*−*25*). In these complexes, the external ligand is located at the sixth position, and interacts with the dissociated His in a similar fashion, as has also been observed for the distal His in Mb and Hb. This suggestion was most recently supported by the publication of the crystal structure of the CO complex of Ngb (*26*). The crystallographic results also showed a drastic structural rearrangement in the heme pocket of Ngb upon CO binding. The rearranged structure might be responsible for the characteristic properties of Ngb in terms of liagnd binding; the affinities of the ligands are basically similar to those observed for Mb and Hb, but the association rates are much faster than in Mb. However, the crystal structure of Cgb in the ferrous CO-bound form is not yet available.

To understand the structure−function relationship of these hexacoordinated heme-containing proteins, it is necessary to examine the arrangement of their active site structures in

detail. In any hemoprotein, the structure of the heme pocket plays a crucial role in controlling protein function, such as heme ligand stability, and thus determines the class of a particular function. In this study, we measured the resonance Raman and IR spectra of the CO- and NO-bound form of Cgb and Ngb in the ferrous form, in an attempt to characterize the structures of their heme environments. The CO and NO adducts have been shown to be useful in investigations of the active sites of hemoproteins, including interactions between the bound ligand and the distal residues. In addition, the proximal environments were characterized using ultrafast picosecond time-resolved resonance Raman (ps-TR^3) spectroscopy to obtain insights into the nature of the Fe−His bond. The Fe−His stretching mode (ν_{Fe-His}), after the photodissociation of CO from the ferrous iron, was examined. These structural data are discussed in relation to the ligand binding properties of Cgb and Ngb. It is of particular interest to compare the structures between the two proteins in detail, since some significant differences have been observed in their ligand binding properties.

EXPERIMENTAL METHODS

Preparation of Recombinant Human Cgb, Ngb, and Their Mutants. The procedures for the expression and purification of human Cgb (*18*) and Ngb (*19*) have been described in detail in previous reports. Mutagenesis was performed on vectors of the wild type (WT) of Cgb and Ngb by PCR. The axial His and/or positively charged residues close to the heme iron were replaced with other residues (H81A, H81V, R84A, R84K, and R84T for Cgb and H64A, H64V, K67A, K67R, and K67T for Ngb) using previously reported vectors, WTCgb-pET15b and WTNgb-pET3a (*18*, *19*), as templates. The sequences of the mutated DNA were determined using a Pharmacia Express sequencer. The expression, purification, and identification of the mutants were the same as those for the WT proteins (*18*, *19*). The concentrations of each recombinant protein was quantified from the heme content, as determined by a pyridine hemochrome assay (*27*). The purified proteins had R_z values (A_{Soret}/A_{280}) of 2.80 for Cgb and 2.95 for Ngb.

Preparation of Ferrous−CO or −NO Adducts of Cgb and Ngb. The proteins were dissolved in a solution containing 50 mM Tris-HCl and 100 mM NaCl buffer (pH 8.0), extensively purged with nitrogen gas, supplemented with sodium dithionite at a final concentration of ∼2 mM, and placed in the cell of a spectrometer. The ferrous−CO form was prepared by treatment with pure CO gas at 1 atm. To remove undesirable oxidized nitrogen species such as NO_2 and N_2O, NO gas was first shaken with 1 N NaOH, and then injected into a Raman cell through a rubber septum with a gastight syringe to produce the ferrous−NO form.

Spectroscopies. ps-TR^3 spectra were obtained using a homemade pump/probe system, as described elsewhere (*28*). Briefly, the probe beam at 442 nm (0.2 μJ/pulse) was generated as the first Stokes stimulated Raman scattering from methane gas, whereas the pump pulse at 540 nm (12 μJ/pulse) was generated with an optical parametric generator and amplifier. Both pulses were obtained by excitation by the second harmonic of the 784 nm output of a Ti-sapphire laser operated at 1 kHz. Raman scattered light was detected with a liquid nitrogen-cooled CCD detector (Roper Scientific, SPEC-10:400B), attached to a single spectrograph (SPEX, model 500M).

Resonance Raman spectra of the CO adducts were obtained using a JASCO NR-1800 spectrometer, equipped with a liquid nitrogen-cooled CCD detector (Princeton Instruments) and operated in the single dispersion mode. The slit width for the spectral measurements was 4 cm^{-1}. An excitation wavelength of 413.1 nm was used and was generated using a Kr^+ laser (Coherent, Innova 90). The laser power was kept at <100 μW at the sample point to prevent photodissociation of the iron-bound CO. The Raman cell was kept spinning to minimize local heating. Optical absorption spectra were routinely measured before and after the resonance Raman measurements of CO adducts for all samples in the Raman cell with a Shimadzu spectrometer (UV-2500PC) using a homemade adaptor. For the ferrous−NO complexes, resonance Raman scattering was excited with the 406.7 nm line of a Kr^+ ion laser (Spectra Physics, model 2016) and was detected by a liquid nitrogen-cooled CCD (Astromed, CCD 3200) attached to a 100 cm single monochromator (Ritsuoyokogaku, DG-100). The Raman excitation beam was introduced from the bottom of the Raman cell, and the radiation scattered along 90° from the incident radiation was collected. The slit width was 200 μm, and the sample temperature was maintained at ∼20 °C. The laser power was kept at <50 μW at the sample point, and the Raman cell was spun at 2000 rpm to avoid photolysis of the coordinated NO and to minimize local heating. Optical absorption spectra were routinely measured before and after the resonance Raman measurements of NO adducts for all samples in the Raman cell with a Hitachi spectrometer (U-3210) using an adaptor. FT-IR spectra of the ferrous−CO complexes were measured using an FT-IR 670 plus instrument (Jasco). Approximately 20 μL of a 2−3 mM protein solution was added to a CaF_2 IR cuvette. All spectra of CO adducts were analyzed by Gaussian band fitting with IGOR Pro4 (WaveMetrics). It was difficult to reliably estimate the ratio of the population of the signal bands by the intensity of ν_{Fe-CO} because the intensity of the ν_{Fe-CO} bands in resonance Raman spectra is dependent on the excitation wavelength (*29*). Thus, the ratio of the population of the signal bands was estimated from the area of the ν_{C-O} in the FT-IR data.

RESULTS

Picosecond-TR^3 Spectra of the CO-Photodissociated Cgb and Ngb. The ps-TR^3 spectra of the CO-photodissociated Cgb and Ngb were measured using 20 and 1000 ps delays after photolysis. In a comparison of the spectra between the CO-bound and CO-photolyzed forms, some new intense lines appeared in the low-frequency region upon photolysis (see the left panels of Figure 2). The lines at 229 cm^{-1} for Cgb and 221 cm^{-1} for Ngb were assigned to Fe−His stretching (ν_{Fe-His}) of the pentacoordinated heme species for these globins in the ferrous high-spin state. Since His113 and His96 were previously assigned as the fifth ligand of the heme iron in CO complexes of Cgb (*18*) and Ngb (*19*), respectively, it seems reasonable to conclude that the ν_{Fe-His} bands for the CO-photolyzed forms of Cgb and Ngb correspond to the stretching modes of the Fe−His113 and Fe−His96 bonds, respectively. In Ngb, a weak and broad ν_{Fe-His} band was previously reported at ∼225 cm^{-1} in the static Raman

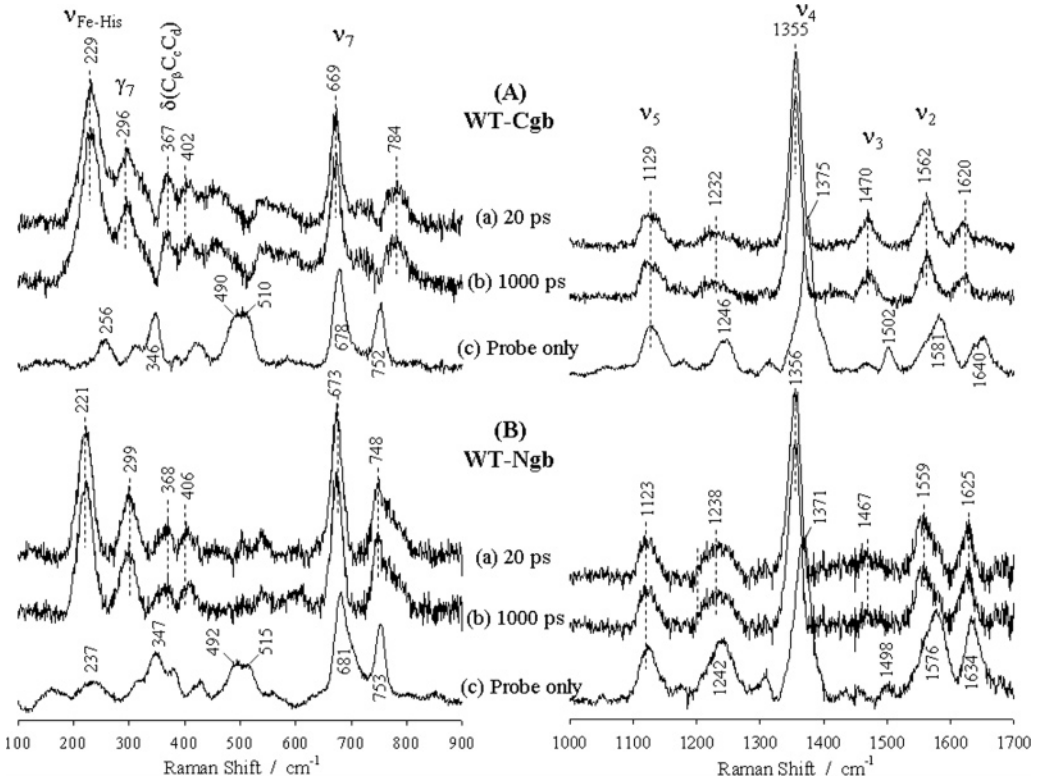

FIGURE 2: ps-TR^3 spectra of CO-photodissociated Cgb and Ngb. Spectra were measured for CO-photodissociated (A) WT-Cgb and (B) WT-Ngb in the low- and high-frequency regions (left and right panels, respectively) at time delays of (a) 20 and (b) 1000 ps. Spectra labeled (c) are the probe only spectra (the ferrous−CO form).

spectrum (*21*), whereas a sharp and well-resolved ν_{Fe-His} band is observed at 221 cm^{-1}, when the ps-TR^3 spectroscopic technique is used. The positions of other lines, i.e., γ_7 (out-of-plane methine wagging), δ ($C_\beta C_c C_d$) (a mode involving the deformation of propionate methylene groups), and ν_7 (breathing-like mode of the porphyrin inner ring) bands (*28*), are also consistent with the electronic and coordination structures of the CO-photolyzed Cgb and Ngb, as described above.

The right panels of Figure 2 show ps-TR^3 spectra in high-frequency regions (1000−1700 cm^{-1}). The spectra contain information concerning heme in-plane vibrations, such as the ν_2 and ν_3 bands (the core size markers), and the ν_4 band (the oxidation state marker) (*30*). The CO-photodissociated Cgb yielded ν_2, ν_3, and ν_4 bands at 1562, 1470, and 1355 cm^{-1}, respectively, while in the CO-bound form, the corresponding bands were at 1581, 1502, and 1375 cm^{-1}, respectively. The CO-photodissociated Ngb produced ν_2, ν_3, and ν_4 bands at 1559, 1467, and 1356 cm^{-1}, respectively, while for the CO-bound form, the bands were located at 1576, 1498, and 1371 cm^{-1}, respectively. The positions of these marker bands for the CO-photolyzed Cgb and Ngb are similar to the positions of the corresponding bands (ν_2 at 1563 cm^{-1} and ν_4 at 1356 cm^{-1}) for their CO-photolyzed Mb form (*28*), whose heme iron is pentacoordinate in the ferrous high-spin state. The vinyl $C_a{=}C_b$ stretching bands at 1640 cm^{-1} for Cgb and at 1634 cm^{-1} for Ngb showed are downshifted upon CO photodissociation. A similar downshift was observed for Mb. On the other hand, no prominent frequency shift was observed for the band at 1129 cm^{-1} of Cgb and the band at 1123 cm^{-1} of Ngb. These bands are assigned to ν_5, a stretching mode of the porphyrin substituent (primarily $\nu_{C_\beta-methyl}$) (*31*). In the case of Mb, the ν_5 band exhibited a downshift upon CO photodissociation: it was observed at 1119 cm^{-1} in the CO-photolyzed form and at 1135 cm^{-1} in the CO-bound form (*28*).

The ps-TR^3 spectral measurements of the CO photolysis of Cgb and Ngb result in two significant and new findings. First, the spectra 1000 ps after the CO photolysis are the same as those after 20 ps, for both Cgb and Ngb. For example, the ν_{Fe-His} band did not exhibit any shift from 20 to 1000 ps after CO photodissociation, which is in sharp contrast to the change in the Raman spectra of Mb (*28*). The ν_{Fe-His} band in Mb shows a downshift from 222 to 220 cm^{-1} with a time constant of ∼100 ps (*28*). The position of the ν_2 frequency (1562 cm^{-1} for Cgb and 1559 cm^{-1} for Ngb) used as the core size marker also did not change from 20 to 1000 ps. This implies that the core size does not change in the picosecond time region. Second, the spectral features of Cgb and Ngb are distinctly different; e.g., the ν_{Fe-His} frequency is different by 8 cm^{-1}. The crystallographic data for Cgb and Ngb in the hexacoordinated heme in the ferric state indicated that the coordination structure of the heme iron is essentially the same (*14*−*17*). Thus, these results suggest that the heme environment, especially the iron coordination structure, would be different between these two globins in the pentacoordinated heme iron in the ferrous high-spin state, which was generated upon CO photodissociation.

IR and Resonance Raman Spectra of CO Adducts of Cgb and Ngb. The heme irons of Cgb and Ngb in the resting ferrous form are in the hexacoordinated state with two His residues as axial ligands. However, exogenous ligands such as O_2, CO, and NO can bind to the heme ferrous iron by replacing one His residue from the sixth coordination position, His81 for Cgb and His64 for Ngb (*18*, *19*). The replaced His residues would act like a "distal His" of Mb.

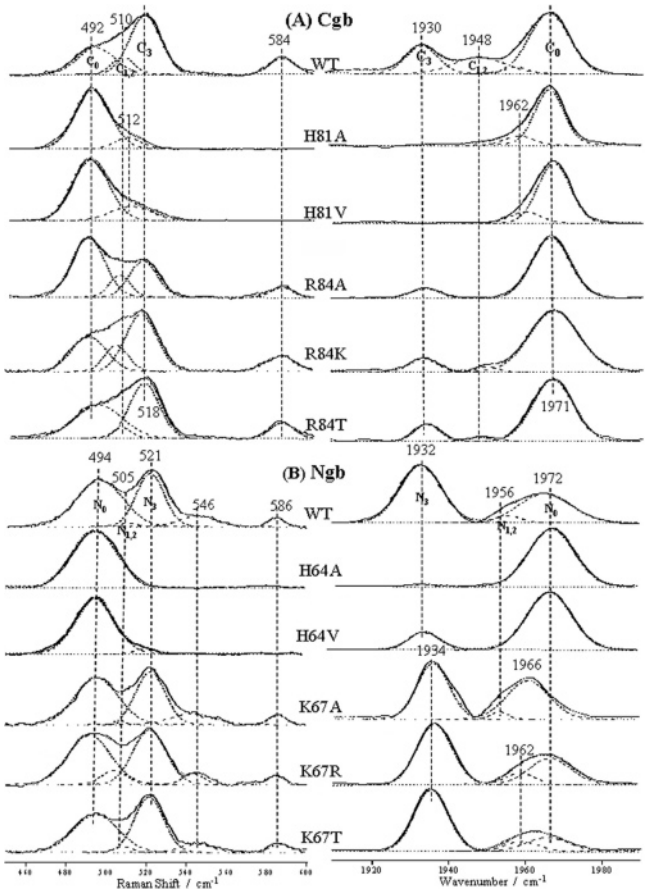

FIGURE 3: Resonance Raman (left panels) and FT-IR (right panels) spectra of (A) Cgb in the ferrous−CO state (from top to bottom, WT, H81A, H81V, R84A, R84K, and R84T) and (B) Ngb of that (from top to bottom, WT, H64A, H64V, K67A, K67R, and K67T).

In addition, Arg84 for Cgb and Lys67 for Ngb are located in the proximity of the sixth coordination position of the heme iron, as has been shown in previous crystallographic studies (*14*−*17*). To examine the nature of the interaction of the iron-bound ligands with the distal residues (His81 and Arg84 for Cgb and His64 and Lys67 for Ngb) in detail, we prepared five distal mutants of Cgb (H81A, H81V, R84A, R84K, and R84T) and five mutants of Ngb (H64A, H64V, K67A, K67R, and K67T). The mutants of Cgb, in which Arg84 was replaced with Lys (R84K) and Thr (R84T), might mimic the active sites of Ngb and Mb, respectively (vice versa for the Ngb mutation).

Figure 3 shows the ν_{Fe-CO} (left panels, resonance Raman spectra) and ν_{C-O} (right panels, FT-IR spectra) frequency regions for the ferrous−CO complexes of (A) Cgb and (B) Ngb, respectively. In the case of WT Cgb (the top spectra in Figure 3A), three sets of ν_{Fe-CO} and ν_{C-O} bands are observed, C_0 (492 cm^{-1}, 1971 cm^{-1}; 60%), $C_{1,2}$ (510 cm^{-1}, 1948 cm^{-1}; 20%), and C_3 (518 cm^{-1}, 1930 cm^{-1}; 20%), in which the percentage values represent the population of each conformer. The (ν_{Fe-CO}, ν_{C-O}) pairs were determined based on a ν_{Fe-CO}−ν_{C-O} correlation plot (*32*), and their populations were estimated on the basis of the area of the ν_{C-O} stretching band by a peak fitting analysis. The Fe−C−O bending mode, δ_{Fe-C-O}, was observed at 584 cm^{-1}. C_0, $C_{1,2}$, and C_3 correspond to conformers of the Mb CO adduct, in which A_0 (491 cm^{-1}, 1965 cm^{-1}; minor), $A_{1,2}$ (∼508 cm^{-1}, 1945 cm^{-1}; 70%), and A_3 (518 cm^{-1}, 1932 cm^{-1}; 30%), respectively, are present (*33*). Upon mutation of His81, the spectral features were drastically changed. A set of ν_{Fe-CO} and ν_{C-O} bands, C_0 (492 cm^{-1}, 1971 cm^{-1}; 90−100%), was mainly present, and the δ_{Fe-C-O} band disappeared. The results clearly suggest that His81, which corresponds to the distal His64 of Mb, interacts sterically and/or electrostatically with the iron-bound CO. On the other hand, the mutation of Arg84 of Cgb did not seriously influence the (ν_{Fe-CO}, ν_{C-O}) positions but affected the population of multiconformers slightly. The spectra of the Arg84 mutants still contained the δ_{Fe-C-O} band. The spectral features of the R84K and R84T mutants of Cgb were not similar to those of Ngb (vide infra) and Mb, respectively, indicating that these mutants of Cgb do not mimic the structures around the heme in Ngb and Mb.

The vibrational spectra of WT Ngb (Figure 3B) produced three sets of ν_{Fe-CO} and ν_{C-O} bands: N_0 (494 cm^{-1}, 1972 cm^{-1}; 40%), $N_{1,2}$ (505 cm^{-1}, 1956 cm^{-1}; 5%), and N_3 (521 cm^{-1}, 1932 cm^{-1}; 55%). The δ_{Fe-C-O} band was observed at 586 cm^{-1}. These spectral features are different from those of Cgb and Mb. However, as in the case of Cgb, the His64 mutation caused a drastic spectral change, suggesting that His64 plays a crucial role in the interaction with iron-bound CO. Unlike Cgb, the Lys67 mutation in Ngb caused a slight shift in the ν_{C-O} frequency of the N_3 and N_0 or $N_{1,2}$ conformer. K67R and K67T mutations did not reproduce the structures of the active site of Cgb and Mb, respectively, as in the case of the swapping mutation of Cgb.

Resonance Raman Spectra of NO Adducts of Cgb and Ngb. Since it was reported that Ngb might be involved in NO-related metabolism during hypoxia (*23*−*25*), we also investigated the Fe−N−O binding characteristics of the ferrous−NO complexes for both globins by static resonance Raman spectroscopy. Figure 4 depicts the resonance Raman spectra of the ferrous−NO adducts of (A) WT Cgb and (B) WT Ngb in the low- and high-frequency regions (left and right panels, respectively). In the low-frequency region of the ^{14}N−^{15}N isotope difference spectra, isotope sensitive bands were observed. According to the assignment for Mb in the ferrous−NO complex, the bands at 569 and 573 cm^{-1} can be assigned to the ν_{Fe-NO} for Cgb and Ngb, respectively, and that at 459 cm^{-1} can be assigned to the Fe−N−O bending mode (δ_{Fe-N-O}) for Cgb. The presence of a single ν_{Fe-NO} band indicates the presence of a single conformer in the ferrous−NO complex for both globins. On the other hand, several isotope sensitive bands were observed around 1600 cm^{-1} in the high-frequency region for the ferrous−NO complexes of Cgb and Ngb. Similar spectral characteristics have previously been observed in the ferrous−NO complex of Mb, and have been explained in terms of the vibrational coupling between the ν_{N-O} band and the porphyrin vibration (*34*, *35*). Thus, these bands can be assigned to the N−O stretching (ν_{N-O}) mode, and the ν_{N-O} frequencies were estimated from their average at 1604 and 1600 cm^{-1} for Cgb and Ngb, respectively.

The ν_{Fe-NO} and ν_{N-O} correlation plot suggests that Cgb and Ngb fall into the class of hemoproteins that contain a hexacoordinate nitrosyl heme (Figure 5). This suggestion is supported by the positions of the ν_4 and ν_3 bands (1376 and 1502 cm^{-1} for Cgb and 1375 and 1498 cm^{-1} for Ngb), which are typical of hexacoordinate heme complexes (*36*). Despite the hexacoordinate iron for Cgb and Ngb, the ν_{N-O} frequencies were lower and the ν_{Fe-NO} frequencies were higher than

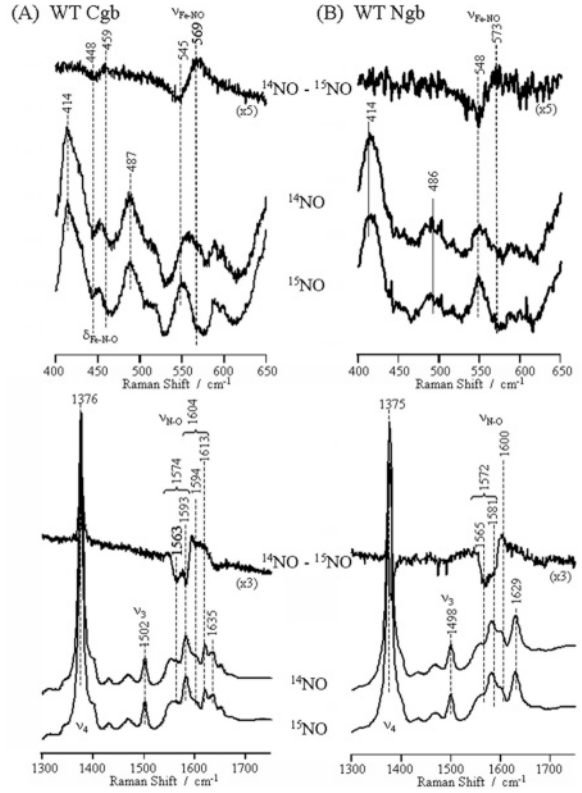

FIGURE 4: Resonance Raman spectra (406.7 nm excitation) in the 400−650 cm^{-1} (top panels) and 1300−1750 cm^{-1} (bottom panels) regions of the ferrous−NO complex of (A) WT Cgb and (B) WT Ngb. From top to bottom: $^{14}N^{16}O - {}^{15}N^{16}O$ difference, $^{14}N^{16}O$, and $^{15}N^{16}O$ spectra.

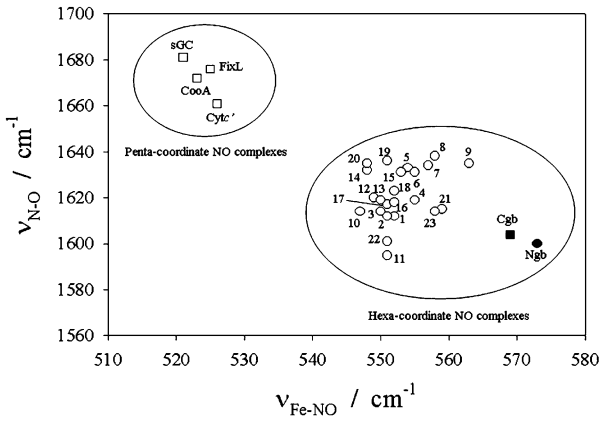

FIGURE 5: Correlation plot between the ν_{Fe-NO} and ν_{N-O} frequencies of various heme proteins. The filled squares and circles represent data for Cgb−NO and Ngb−NO adducts, respectively. The empty squares represent data for pentacoordinate NO complexes, and the empty circles represent data for Mb: 1, human WT; 2, pig WT; 3, sperm whale WT; 4, human H64Q; 5, human H64G; 6, human H64A; 7, human H64V; 8, human H64I; 9, human H64L; 10, sperm whale V68S; 11, pig V68N; 12, human V68G; 13, human V68A; 14, human V68T; 15, pig H64V/V68T; 16, sperm whale F46W; 17, sperm whale F46L; 18, sperm whale F46V; 19, sperm whale F46A; 20, sperm whale F46I; 21, sperm whale L29W; 22, sperm whale L29F; and 23, sperm whale L29F/H64Q. Data for 1−23 were obtained from ref *35*. Abbreviations: sGC, soluble guanylate cyclase; Cyt *c*′, cytochrome *c*′.

the corresponding values for Mb (ν_{N-O} = 1612 cm^{-1}, ν_{Fe-NO} = 552 cm^{-1}) (*34*, *35*). The Fe−NO bond in Cgb and Ngb was somewhat stronger than that in Mb. Eventually, the ν_{Fe-NO} bands of Cgb and Ngb were very close to the ν_{Fe-OO} frequencies (572 cm^{-1} for Cgb and 571 cm^{-1} for Ngb) of their O_2 complexes, in contrast to the observation for Mb (ν_{Fe-OO} = 569 cm^{-1}) (*37*).

DISCUSSION

In the study presented here, the structures in the heme environment of Cgb and Ngb for the CO- or NO-bound and CO-photodissociated forms were characterized. In the CO- and NO-bound forms, the CO or NO ligand occupies the sixth coordination site after expelling the endogenous His ligand from its original position. In the CO-photodissociated forms, the heme iron is pentacoordinate with a vacant sixth position. The vibrational spectra of these forms of Cgb and Ngb obtained in this study clearly show structural differences in the heme environment among Cgb, Ngb, and Mb. The differences might be responsible for the differences in ligand binding kinetics and equilibria.

Structural Properties of the Heme Proximal Side. We successfully detected the ν_{Fe-His} band of Cgb and Ngb using the ps-TR^3 spectroscopic technique. The ν_{Fe-His} bands for various hemoproteins have been observed in the 200−260 cm^{-1} region (*38*), and it is well-known that the frequencies are influenced by the hydrogen bonding status of the proximal His imidazole and steric distortion in the Fe−His linkage. It is also noteworthy that the ν_{Fe-His} frequencies are closely associated with activities at the sixth iron site, that is, the physiological activities of hemoproteins. For example, the Fe−His bond in gas-sensing hemoproteins is exerted by steric strain, eventually providing lower ν_{Fe-His} frequencies than other hemoproteins. The relatively weak Fe−His bond is functionally attributable to intramolecular signal transduction by sensor hemoproteins via conformation changes, which are initiated by the dissociation of the axial ligand from the iron sixth site (*39*). In contrast, the strong Fe−His bonds of peroxidases, resulting from a strong hydrogen bond of the His imidazolyl NH with its surroundings (e.g., carboxylate), give high ν_{Fe-His} frequencies, and substantially contribute to the heterolytic cleavage of the peroxide O−O bond at the sixth position through an electron pushing effect (*40*).

The ν_{Fe-His} frequencies of Cgb (229 cm^{-1}) and Ngb (221 cm^{-1}) fall into the range of those observed for the globin family (ca. 220 cm^{-1}), suggesting that the physiological activities of Cgb and Ngb are similar to those of other globins such as Mb and Hb, i.e., ligand (O_2) binding at the sixth coordination position. However, some differences were observed in the ν_{Fe-His} position between Cgb and Ngb, and Mb. In addition, the ν_{Fe-His} band exhibited no time-dependent shift from 20 to 1000 ps after CO photodissociation. In the case of Mb, the shift in the ν_{Fe-His} band from 222 to 220 cm^{-1} with a time constant of ~100 ps can be explained in terms of protein conformational relaxation in the heme proximal side, after CO dissociation from the sixth site (*28*). After CO dissociation, the iron would move out of the porphyrin plane within several picoseconds, but some steric strain would be retained in the heme proximal side, especially at the Fe−His bond, which would be released in the 100 ps time domain. We therefore suggest that the structural relaxation in the heme proximal side in Cgb and Ngb after CO photolysis would be rather small or faster than the picosecond time domain. This conclusion is supported by the mutation effect of the distal His in Cgb and Ngb on the spectra, in which the ν_{Fe-His} band of the WT globins observed

in the TR[3] spectra exactly coincides with those observed in the static resonance Raman spectra of the H81A mutant of Cgb (228 cm^{-1}, data not shown) and the H64V mutant of Ngb (221 cm^{-1}, ref *19*). Since these mutants in the deoxy state can be considered models of the fully relaxed state for each globin after CO dissociation, the spectral similarities suggest that the conformational relaxation in the proximal side is complete within 20 ps. That is, the Fe−His linkage would not be sterically tensed in Cgb and Ngb in the CO-bound form. As evidenced by the absence of a shift of the ν_2 band of Cgb (1562 cm^{-1}) and Ngb (1559 cm^{-1}), the core size expansion would be also completed immediately after CO photolysis. On the basis of the differences of the ν_{Fe-His} frequency and of its relaxation process, it appears that the structure in the heme proximal side of the hexacoordinated globins (Cgb and Ngb) is different from that of the pentacoordinated globin (Mb).

However, as shown in Figure 1, structural comparisons of the heme environment of (A) ferric Cgb, (B) ferric Ngb, and (C) deoxyMb indicate that the proximal His $N^{\delta 2}$ atom for these globins interacts with the oxygen atom of the main chain carbonyl group (Val109 for Cgb, Leu92 for Ngb, and Leu89 for Mb). The structural characteristics are basically similar among these globins. Thus, it is thought that the structures in the heme environment of Cgb and Ngb must be altered upon association of CO with the heme ferrous iron. Recently, Nienhaus and co-workers reported the crystal structure of the CO-bound form of Ngb. There were substantial structural differences between the CO-bound and the ferric resting forms (*26*). Once CO binds, the heme plane slides from the original (ferric) position, resulting in the elongation of the Fe−His bond from 2.12 Å (ferric state, PDB entry 1OJ6) to 2.24 Å (ferrous−CO state, PDB entry 1W92). This heme sliding movement would be toward the cavity observed in the proximal side of the ferric form, eventually inducing a topological reorganization of the large internal cavity and the connectivity of the heme cavity with the bulk. It seems to be reasonable to expect such a structural change for Cgb (sliding motion of the heme plane) upon CO binding, although the crystal structure of its CO complex is not yet available. However, the structural change must be somewhat different between Cgb and Ngb, because the cavity located in the heme proximal side of Cgb is substantially different in size and position from that in Ngb. For example, while the large internal cavity for the movement of Phe106, which accompanied the heme sliding motion, is observed in the heme proximal side of Ngb, the corresponding position is occupied by Val162 in Cgb (see Figure 1). Thus, there is a little room in Cgb for heme sliding caused by CO binding. The structures of the CO-photodissociated forms of Cgb and Ngb would reflect those of their CO-bound forms stated above: the resulting Fe−His bond is stronger in Cgb than in Ngb.

The intensity of the observed ν_{Fe-His} bands for Cgb and Ngb is relatively large compared to that for Mb and HbA. Bangcharoenpaurpong et al. (*41*) found that the Fe−His stretching vibration is relatively strongly coupled to the Soret transition. Their hypothesis is that the origin of the resonance Raman intensity of the Fe−His vibrational mode results from the orbital overlap between the σ^* orbital of the Fe−His bond ($\sigma^*_{Fe-NHis}$) and the π^* orbital of the porphyrin ring (π^*_{por}), which is small in the planar structure but becomes large in the nonplanar structure. The Fe−His configuration is defined by (1) the out-of-plane displacement of the Fe atom caused by ligand photodissociation (defined as the distance from the average plane of the porphyrin ring), (2) the tilt angle of the Fe−His bond (relative to the heme normal), and (3) the azimuthal angle (about the heme normal). The $\pi_{por}-\pi^*_{por}$ excitation can result in direct harmonic coupling of the $Fe-N_{His}$ mode via the orbital mixing of π^*_{por} and $\sigma^*_{Fe-NHis}$. The stronger this coupling, the higher the resonance Raman intensity of the Fe−His stretching mode upon Raman excitation into the Soret band. The band intensity of the ν_{Fe-His} mode increases with increasing out-of-plane displacement of the iron, because of the increased orbital overlap between $\sigma^*_{Fe-NHis}$ and π^*_{por}. The theoretical model by Stavrov et al. also pointed out that out-of-plane displacement of the iron gives rise to intensity and frequency changes in the ν_{Fe-His} band due to the orbital mixing of π^*_{por} with $\sigma^*_{Fe-NHis}$ (*42*). The observed strong ν_{Fe-His} bands suggest that the hemes of both proteins have large out-of-plane displacements of the iron in the picosecond time region after CO dissociation.

It should be noted that the Fe−NO stretching (ν_{Fe-NO}) frequency for the ferrous−NO complex was lower in Cgb (569 cm^{-1}) than in Ngb (573 cm^{-1}), although the ν_{N-O} band is located at the same position ($\sim$1600 cm^{-1}) in these two globins (see Figure 4). The vibrational properties of the Fe−NO unit are modulated by factors that are distinctly different from the case for the Fe−CO unit; the nature of the heme proximal ligand sensitively affects the Fe−NO mode, but the polarity of the distal pocket has no influence on the Fe−NO mode (*34, 43*). Under their theories, the Fe−NO bond strength of Cgb is weaker than that of Ngb. It is likely that the Fe−His bond in the ferrous state is stronger in Cgb than in Ngb, which is in good agreement with the results of the ν_{Fe-His} mode.

Structural Properties of the Heme Distal Side. As stated above, the binding of CO to Cgb and Ngb induces a structural rearrangement in the heme pocket. The rearranged structure could be reflected in the Fe−CO and C−O stretching modes of Cgb and Ngb, as reported herein. In the vibrational spectra of Cgb and Ngb, the multiple ν_{Fe-CO} and ν_{C-O} bands are indicative of the presence of three conformers with respect to the Fe−CO moieties in the rearranged structure. Their positions and populations were affected by mutations of the distal residues. In this study, three findings concerning the conformers arose. First, a spectral comparison of the swapping mutations, Ngb (K67R) versus Cgb (R84K), Mb versus Ngb (K67T), and Mb versus Cgb (R84T), suggests that the heme environmental structures of Cgb and Ngb in the CO-binding form are entirely different from that of Mb. The findings also suggest the existence of some structural difference in the heme distal side between Cgb and Ngb. Second, the distal His (His64 in Ngb and His81 in Cgb) plays crucial roles in the binding of CO to these globins, because the population of the conformers was drastically changed upon mutation of this His (details will be discussed in the paragraph below). The Fe−C−O bending mode (δ_{Fe-C-O}) could be observed in the presence of the distal His but disappeared upon replacement of the distal His with Ala or Val. In contrast to the bent or tilt coordination of the CO ligand in the WT globins, the linear coordination is favorable for these His mutants, suggesting that His81 for Cgb and His64 in Ngb affect the CO coordination through steric as well as electrostatic interactions. Third, Arg84 in Cgb and

Lys67 in Ngb are not significantly involved in interactions with the CO ligand. The population of the conformer is changed in the Arg84 mutant of Cgb and in the Lys67 mutant of Ngb. These observations can be attributed to a hydrophobic effect of the Ala or Val side chain, but the effect is not so serious as that from the distal His. The location of these residues might be changed due to the structural rearrangement that occurs from the ferric to the CO-bound form.

In the multiple conformations of the CO complexes, the ν_{Fe-CO} and ν_{C-O} frequencies are similar among the three globins. Thus, the structure of each conformer in Cgb and Ngb appears to be similar to the corresponding one in Mb. However, population of each conformer was different among the three globins. On the basis of these data, the structure of each conformer in Cgb and in Ngb can be discussed in comparison with those in Mb because the structure of the Mb conformers has been comprehensively discussed. C_0 in Cgb and N_0 in Ngb provide the ν_{Fe-CO} and ν_{C-O} bands at ~490 and ~1970 cm^{-1}, respectively. On the basis of the results of experiments with the mutated proteins, it is likely that the distal His is not involved in this conformation. The spectral properties of this conformer are comparable to those of A_0 in Mb, the ν_{Fe-CO} and ν_{C-O} of which are located at 491 and 1965 cm^{-1}, respectively. In the case of Mb, the distal His residue in the A_0 conformation is swung out from the heme pocket to enhance the solvation of the positive charge, leaving a hydrophobic and/or a negative electric field in the heme pocket, the so-called "open" state. Thus, the A_0 open conformer is minor at neutral pH, while it is dominant at acidic pH. Accordingly, C_0 and N_0 can be attributed to the open conformer in Cgb and Ngb, respectively. Even at neutral pH, the open conformer occurs in a higher proportion, the population of which is 60 and 40% for Cgb and Ngb, respectively. This spectral finding is consistent with the crystallographic results for the CO complex of Ngb: the heme distal pocket was found to connect to the solvent region in the crystalline state.

On the other hand, C_3 and N_3 whose ν_{Fe-CO} and ν_{C-O} appear at ~520 and ~1930 cm^{-1}, respectively, could be assigned to the "closed" conformer, as in the case of A_3 of Mb. Since the iron-bound CO in A_3 is surrounded by a H-bonding residue(s) and/or a positive electric field, the distal His in Cgb and Ngb possibly interacts with the iron-bound CO, but the conformation of this conformer has not yet been observed in the crystal structure of Cgb and Ngb. $C_{1,2}$ and $N_{1,2}$ (ν_{Fe-CO} ~ 510 cm^{-1} and ν_{C-O} ~ 1950 cm^{-1}) could correspond to $A_{1,2}$ of Mb, which is an intermediate state of the conformer between A_0 and A_3. Although the $A_{1,2}$ population of Mb is major (70%) at neutral pH, $C_{1,2}$ and $N_{1,2}$ are very minor in Cgb (20%) and in Ngb (5%).

Relationship between the Heme Environmental Structure and Ligand Binding. The binding of exogenous ligands to globins has been extensively studied in relation to the dynamic interconversion between multiple conformers. For example, mutants of Mb, in which the open conformer was dominant, exhibited a faster association with the ligand than WT Mb. As in the case of Mb, the distal His is also involved in such an interconversion of conformers in both Cgb and Ngb. However, different from Mb, the open conformer (C_0 and N_0) for exogenous ligand binding is predominant in the case of Cgb and Ngb. This is the main reason ligand association of Cgb and Ngb is faster than that of Mb, as observed in flash photolysis experiments (*8*, *44*). A similar explanation has been made for the CO complex of murine Ngb on the basis of its crystal structure (*26*); the sixth ligand site was discussed in relation to the influence of the volume and position in the heme cavity and steric and/or electostatic effect(s) in the distal heme pocket upon ligand binding.

A comparison of the vibrational spectra between Cgb and Ngb leads us to expect that the ligand association rate might be faster in Cgb than in Ngb because the open conformer is present at higher concentrations in Cgb (C_0, 60%) than in Ngb (N_0, 40%). However, the rate constants for association of Ngb with O_2 ($k_{on}^{O_2} = 130\ \mu M^{-1}\ s^{-1}$) and CO ($k_{on}^{CO} = 38\ \mu M^{-1}\ s^{-1}$) are larger than the corresponding values ($k_{on}^{O_2} = 30\ \mu M^{-1}\ s^{-1}$, $k_{on}^{CO} = 5.6\ \mu M^{-1}\ s^{-1}$) of Cgb (*8*, *44*). This incompatibility might be explainable by incorporating other factors that control ligand binding to Cgb and Ngb. Champion and co-workers recently found that the k_{on}^{CO} rate constants of Mb mutants with a weaker Fe−X bond (e.g., H93G-dibromopyridine, -imidazole, -pyridine, and -4-bromoimidazole, where X is a fifth ligand) are higher than those of WT Mb, based on the proposal that the Fe−His bond strength has a significant influence on the kinetics of binding of the diatomic ligand to the heme iron (k_{on}) (*45*). If this notion were applied to our case and it is assumed that the Fe−His bond is stronger in Cgb than in Ngb, which is supported by the kinetic results, the ligand association would be expected to be slower in Cgb than in Ngb.

In summary, the heme environmental structures of Cgb and Ngb in the ligand-bound (Fe^{2+} low-spin) and ligand-dissociated (Fe^{2+} high-spin) forms were characterized, and the findings are discussed in relation to their ligand binding properties. In these cases, ligand binding could be controlled by both the distal structure and the proximal ligand, in association with the dynamic motion of the protein part. This might be related to the physiological function of Cgb and Ngb, such as O_2 sensing and/or signal transduction.

ACKNOWLEDGMENT

We are grateful to Prof. Shinya Yoshikawa and Dr. Masao Mochizuki (University of Hyogo) for FT-IR measurements.

REFERENCES

1. Hardison, R. C. (1996) A Brief History of Hemoglobin: Plant, Animal, Protist, and Bacteria, *Proc. Natl. Acad. Sci. U.S.A. 93*, 5675−5679.
2. Dickerson, R. E., and Geis, I. (1983) *Hemoglobin: Structure, Function, Evolution and Pathology*, Benjamin/Cummings, Menlo Park, CA.
3. Flögel, U., Merx, M. W., Gödecke, A., Decking, U. K., and Schrader, J. (2001) Myoglobin: A Scavenger of Bioactive NO, *Proc. Natl. Acad. Sci. U.S.A. 98*, 735−740.
4. Burmester, T., Weich, B., Reinhardt, S., and Hankeln, T. (2000) A Vertebrate Globin Expressed in the Brain, *Nature 407*, 520−523.
5. Burmester, T., Ebner, B., Weich, B., and Hankeln, T. (2002) Cytoglobin: A Novel Globin Type Ubiquitously Expressed in Vertebrate Tissues, *Mol. Biol. Evol. 19*, 416−421.
6. Kawada, N., Kristensen, D. B., Asahina, K., Nakatani, Y., Minamiyama, Y., Seki, N., and Yoshizato, K. (2001) Characterization of a Stellate Cell Activation-associated Protein (STAP) with Peroxidase Activity Found in Rat Hepatic Stellate Cells, *J. Biol. Chem. 276*, 25318−25323.
7. Nakatani, K., Okuyama, H., Himahara, Y., Saeki, S., Dong-Ho Kim, Nakajima, Y., Seki, S., Kawada, N., and Yoshizato, K. (2003) Cytoglobin/STAP, its unique localization in splanchnic fibroblast-like cells and function in organ fibrogenesis, *Lab. Invest. 84*, 91−101.

8. Trent, J. T., III, and Hargrove, M. S. (2002) A Ubiquitously Expressed Human Hexacoordinate Hemoglobin, *J. Biol. Chem. 277*, 19538−19545.
9. Schmidt, M., Giessl, A., Laufs, T., Hankeln, T., Wolfrum, U., and Burmester, T. (2003) How Does the Eye Breathe? Evidence for Neuroglobin-mediated Oxygen Supply in the Mammalian Retina, *J. Biol. Chem. 278*, 1932−1935.
10. Pesce, A., Bolognesi, M., Bocedi, A., Ascenzi, P., Dewilde, S., Moens, L., Hankeln, T., and Burmester, T. (2002) Neuroglobin and Cytoglobin. Fresh Blood for the Vertebrate Globin Family, *EMBO Rep. 3*, 1146−1151.
11. Fordel, E., Geuens, E., Dewilde, S., Rottiers, P., Carmeliet, P., Grooten, J., and Moens, L. (2004) Cytoglobin Expression Is Upregulated in All Tissues Upon Hypoxia: An in Vitro and in Vivo Study by Quantitative Real-time PCR, *Biochem. Biophys. Res. Commun. 319*, 342−348.
12. Sun, Y., Jin, K., Mao, X. O., and Zhu, D. A. (2001) Neuroglobin Is Up-regulated by and Protects Neurons from Hypoxic-ischemic Injury, *Proc. Natl. Acad. Sci. U.S.A. 98*, 15306−15311.
13. Brunori, M., Giuffrè, A., Nienhaus, K., Nienhaus, G. U., Scandurra, F. M., and Vallone, B. (2005) Neuroglobin, Nitric Oxide, and Oxygen: Functional Pathways and Conformational Changes, *Proc. Natl. Acad. Sci. U.S.A. 102*, 8483−8488.
14. Pesce, A., Dewilde, S., Nardini, M., Moens, L., Ascenzi, P., Hankeln, T., Brumester, T., and Bolognesi, M. (2003) Human Brain Neuroglobin Structure Reveals a Distinct Mode of Controlling Oxygen Affinity, *Structure 11*, 1087−1095.
15. de Sanctis, D., Dewilde, S., Pesce, A., Moens, L., Ascenzi, P., Hankeln, T., and Bolognesi, M. (2004) Crystal Structure of Cytoglobin: The Fourth Globin Type Discovered in Man Displays Heme Hexa-coordination, *J. Mol. Biol. 336*, 917−927.
16. Sugimoto, H., Makino, M., Sawai, H., Kawada, N., Yoshizato, K., and Shiro, Y. (2004) Structural Basis of Human Cytoglobin for Ligand Binding, *J. Mol. Biol. 339*, 873−885.
17. Vallone, B., Nienhaus, K., Brunori, M., and Nienhaus, G. U. (2004) The Structure of Murine Neuroglobin: Novel Pathways for Ligand Migration and Binding, *Proteins 56*, 85−92.
18. Sawai, H., Kawada, N., Yoshizato, K., Nakajima, H., Aono, S., and Shiro, Y. (2003) Characterization of the Heme Environmental Structure of Cytoglobin, a Fourth Globin in Humans, *Biochemistry 42*, 5133−5142.
19. Uno, T., Ryu, D., Tsutsumi, H., Tomisugi, Y., Ishikawa, Y., Wilkinson, A. J., Sato, H., and Hayashi, T. (2004) Residues in the Distal Heme Pocket of Neuroglobin, *J. Biol. Chem. 279*, 5886−5893.
20. Dewilde, S., Kiger, L., Burmester, T., Hankeln, T., Baudin-Creuza, V., Aerts, T., Marden, M. C., Caubergs, R., and Moens, L. (2001) Biochemical Characterization and Ligand Binding Properties of Neuroglobin, a Novel Member of the Globin Family, *J. Biol. Chem. 276*, 38949−38955.
21. Couture, M., Brumester, T., Hankeln, T., and Rousseau, D. L. (2001) The Heme Environment of Mouse Neuroglobin, *J. Biol. Chem. 276*, 36377−36382.
22. Kriegl, J. M., Bhattacharyya, A. J., Nienhaus, K., Deng, P., Minkow, O., and Nienhaus, G. U. (2002) Ligand binding and protein dynamics in neuroglobin, *Proc. Natl. Acad. Sci. U.S.A. 98*, 15306−15311.
23. Van Doorslaer, S., Dewilde, S., Kiger, L., Nistor, S. V., Goovaerts, E., Mardon, M. C., and Moens, L. (2003) Nitric Oxide Binding Properties of Neuroglobin: A Characterization by EPR and Flash Photolysis, *J. Biol. Chem. 278*, 4919−4925.
24. Trandafir, F., Van Doorslaer, S., Dewilde, S., and Moens, L. (2004) Temperature Dependence of NO Binding Modes in Human Neuroglobin, *Biochim. Biophys. Acta 1702*, 153−161.
25. Herold, S., Fago, A., Weber, R. E., Dewilde, S., and Moens, L. (2004) Reactivity Studies of the Fe(III) and Fe(II)NO Forms of Human Neuroglobin Reveal a Potential Role against Oxidative Stress, *J. Biol. Chem. 279*, 22841−22847.
26. Vallone, B., Nienhaus, K., Matthes, A., Brunori, M., and Nienhaus, G. U. (2004) The Structure of Carbonmonoxy Neuroglobin Reveals a Heme-sliding Mechanism for Control of Ligand Affinity, *Proc. Natl. Acad. Sci. U.S.A. 101*, 17351−17356.
27. Berry, E. A., and Trumpower, B. L. (1987) Simultaneous Determination of Heme a, b, and c from Pyridine Hemochrome Spectra, *Anal. Biochem. 161*, 1−15.
28. Mizutani, Y., and Kitagawa, T. (2001) Ultrafast Structural Relaxation of Myoglobin Following Photodissociation of Carbon Monoxide Probed by Time-resolved Resonance Raman Spectroscopy, *J. Phys. Chem. B 105*, 10992−10999.
29. Li, Z., Pal, B., Takenaka, S., Tsuyama, S., and Kitagawa, T. (2005) Resonance Raman Evidence for the Presence of Two Heme Pocket Conformations with Varied Activities in CO-Bound Bovine Soluble Guanylate Cyclase and Their Conversion, *Biochemistry 44*, 939−946.
30. Spiro, T. G., and Li, X.-Y. (1988) Resonance Raman Spectroscopy of Metalloporphyrins, in *Biological Applications of Raman Spectroscopy* (Spiro, T. G., Ed.) Vol. III, pp 1−37, John Wiley & Sons, New York.
31. Hu, S., Smith, K. M., and Spiro, T. G. (1996) Assignment of Protoheme Resonance Raman Spectrum by Heme Labeling in Myoglobin, *J. Am. Chem. Soc. 118*, 12638−12646.
32. Yu, N.-T., and Kerr, E. A. (1988) Vibrational Modes of Coordinated CO, CN^-, O_2, and NO, in *Biological Applications of Raman Spectroscopy* (Spiro, T. G., Ed.) Vol. III, pp 39−96, John Wiley & Sons, New York.
33. Ling, J., Li, T., Olson, J. S., and Bocian, D. F. (1994) Identification of the iron−carbonyl stretch in distal histidine mutants of carbonmonoxy myoglobin, *Biochim. Biophys. Acta 1188*, 417−421.
34. Tomita, T., Hirota, S., Ogura, T., Olson, J. S., and Kitagawa, T. (1999) Resonance Raman Investigation of Fe−N−O Structure of Nitrosylheme in Myoglobin and Its Mutants, *J. Phys. Chem. B 103*, 7044−7054.
35. Coyle, C. M., Vogel, K. M., Rush, T. S., III, Kozlowski, P. M., Williams, R., Dou, Y., Ikeda-Saito, M., Olson, J. S., Zgierski, M. Z., and Spiro, T. G. (2003) FeNO Structure in Distal Pocket Mutants of Myoglobin Based on Resonance Raman Spectroscopy, *Biochemistry 42*, 4896−4903.
36. Benko, B., and Yu, N.-T. (1983) Resonance Raman Studies of Nitric Oxide Binding to Ferric and Ferrous Hemoproteins: Detection of Fe(III)−NO Stretching, Fe(III)−N−O bending, and Fe(II)−N−O Bending Vibrations, *Proc. Natl. Acad. Sci. U.S.A. 80*, 7042−7046.
37. Jeyarajah, S., Proniewicz, L. M., Bronder, H., and Kincaid, J. R. (1994) Low-Frequency Vibrational Modes of Oxygenated Myoglobin, Hemoglobin, and Modified Derivatives, *J. Biol. Chem. 269*, 31047−31050.
38. Kitagawa, T. (1988) The Heme Protein Structure and the Iron Histidine Stretching Mode, in *Biological Applications of Raman Spectroscopy* (Spiro, T. G., Ed.) Vol. III, pp 99−131, John Wiley & Sons, New York.
39. Deinum, G., Stone, J. R., Babcock, G. T., and Marletta, M. A. (1996) Binding of Nitric Oxide and Carbon Monoxide to Soluble Guanylate Cyclase As Observed with Resonance Raman Spectroscopy, *Biochemistry 35*, 1540−1547.
40. Smulevich, G., Mauro, J. M., Fishel, L. A., English, A. M., Kraut, J., and Spiro, T. G. (1988) Heme pocket interactions in cytochrome *c* peroxidase studied by site-directed mutagenesis and resonance Raman spectroscopy, *Biochemistry 27*, 5477−5485.
41. Bangcharoenpaurpong, O., Schomacker, K. T., and Champion, P. M. (1984) Resonance Raman Investigation of Myoglobin and Hemoglobin, *J. Am. Chem. Soc. 106*, 5688−5698.
42. Stavrov, S. S. (1993) The Effect of Iron Displacement Out of the Porphyrin Plane on the Resonance Raman Spectra of Heme Proteins and Iron Porphyrins, *Biophys. J. 65*, 1942−1950.
43. Vogel, K. M., Kozlowski, P. M., Zgierski, M. Z., and Spiro, T. G. (1999) Determinants of the FeXO (X = C, N, O) Vibrational Frequencies in Heme Adducts from Experiment and Density Functional Theory, *J. Am. Chem. Soc. 121*, 9915−9921.
44. Trent, J. T., III, Watts, R. A., and Hargrove, M. S. (2001) Human Neuroglobin, a Hexacoordinate Hemoglobin that Reversibly Binds Oxygen, *J. Biol. Chem. 276*, 30106−30110.
45. Cao, W., Ye, X., Sjodin, T., Christian, J. F., Demidov, A. A., Berezhna, S., Wang, W., Barrick, D., Sage, J. T., and Champion, P. M. (2004) Investigations of Photolysis and Rebinding Kinetics in Myoglobin Using Proximal Ligand Replacements, *Biochemistry 43*, 11109−11117.
46. Kraulis, P. J. (1991) MOLSCRIPT: A program to Produce Both Detailed and Schematic Plots of Protein Structures, *J. Appl. Crystallogr. 24*, 946−950.
47. Merritt, E. A., and Bacon, D. J. (1997) Raster3D: Photo-realistic Molecular Graphics, *Methods Enzymol. 277*, 505−524.

BI050997O